

Article

Functionalized Surface Layer on Poplar Wood Fabricated by Fire Retardant and Thermal Densification. Part 1: Compression Recovery and Flammability

Demiao Chu ^{1,2}, Jun Mu ^{2,*}, Stavros Avramidis ³, Sohrab Rahimi ³, Shengquan Liu ¹ and Zongyuan Lai ²

¹ School of Forestry and Landscape Architecture, Anhui Agricultural University, Hefei 230036, China; 13chudemiao@sina.cn (D.C.); liusq@ahau.edu.cn (S.L.)

² Key Laboratory of Wood Material Science and Utilization (Beijing Forestry University), Ministry of Education, Beijing 100083, China; lzy2015@bjfu.edu.cn

³ Department of Wood Science, University of British Columbia, Vancouver, BC V6T 1Z4, Canada; stavros.avramidis@ubc.ca (S.A.); sohrab.rahimi@alumni.ubc.ca (S.R.)

* Correspondence: mujun@bjfu.edu.cn; Tel.: +86-010-62336053

Received: 9 October 2019; Accepted: 23 October 2019; Published: 26 October 2019



Abstract: To enhance compression stability and fire retardancy of densified wood, a new modification method i.e., combined nitrogen–phosphorus (NP) fire retardant pre-impregnation with surface thermo-mechanical densification is used to fabricate a certain thickness of functionalized surface layer on poplar. This combined treated wood is investigated via vertical density profile (VDP), and the compression stability is revealed by both soaking test and cone analysis. Results demonstrate that the combined treatment hardened the surface of wood and reformed the interface combination of the NP with the wood cell wall, thus making the surface tissue more close-grained. Fire retardancy was also enhanced; the total heat release and CO generation values decreased by 21.9% and 68.4%, respectively, when compared with that of solely NP-treated wood. Moreover, surface hardness increased by 15.8%, and the recovery of surface hardness and thickness were 56.8% and 77.2% lower than that of simply densified wood. It appears that this NP-involved thermal densification could be considered as an alternative approach to enhance both the compression stability and fire resistance of wood.

Keywords: wood; fire retardancy; heat treatment; compression recovery; surface layer

1. Introduction

Wood has been considered as one natural composite material for a long time, and it is one of the most popular materials in construction, interior decoration, and the furniture industry mainly because of its strength-to-weight ratio, renewability, and versatility [1]. Furthermore, small-diameter timbers or some remains can be transformed into particles or fibers, which are commonly used to manufacture different composites with other materials like polymers, cement, etc. [2,3].

Since the conservation mandates for natural forests were improved in China, the demand for plantation trees such as poplar, eucalypt, and pine has increased, making them a reliable alternative for industrial timbers [4,5]. Nevertheless, the drawback of using plantation timbers is mostly related to their low density, mechanical strength, and dimensional stability [6]. Densification has been reported for over a century as an efficient method for enhancing wood mechanical properties by reducing porosity and increasing density [7]. Densification is proven to improve mechanical properties such as modulus of elasticity (MOE), surface hardness, and mechanical strength of wood, especially for low-density

species [8]. Song et al. (2018) successfully created a high-performance structural compressed wood via partial removal of lignin and hemicellulose and hot-pressing into highly aligned cellulose nanofibers, resulting in specific strength higher than that of most structural metals and alloys [9].

The conventional wood densification is usually carried out by thermo-mechanical (TM) or thermo-hydro-mechanical (THM) means [3,10]. Büyüksarı found that the thermally compressed veneer could be used to laminate with MDF panels for structural purposes due to the improvement of hardness [8]. Nonetheless, the wood is incompletely densified and the state of compression of TM/THM wood is sensitive to moisture and temperature that could cause utilization problems [7,11,12]. Researchers have studied different methods such as resin pre-impregnation, steam treatment, microwave treatment, and pre-acetylation in order to improve the compression stability of densified wood [13–15].

Recently, researchers focused on the combined effects of heat treatment (HT) and wood densification on the assumption that the post-thermal treatment could release the inner stresses and increase the stability of the compressed wood [8,16]. HT has been employed at various temperatures (160–260 °C) and various media reactions such as vacuum, nitrogen, steam, or oil [17,18]. Heat-treated wood (W_{HT}) relatively enhanced dimensional stability, biological resistance, and aesthetic characteristics [19–22]. The degradation of hemicellulose, conformational arrangement changes of wood biopolymers, and the plasticization of lignin during HT could result in lower number of hydrophilic groups and, consequently, improved dimensional stability [20,23,24]. Fang et al. (2011, 2012) combined oil-heat treatment with wood densification and claimed that the HT could efficiently improve dimensional stability, mechanical properties, and compression set recovery of THM densified veneers [25,26]. Avila et al. (2012) studied selected properties of THM wood using nano-indentations analysis and found an improvement of mechanical properties attributed to an increase in wood density. Furthermore, they reported an increase in the mechanical properties of the cell wall [27]. Zhan and Avramidis (2016) investigated the equilibrium moisture content and radial swelling strain ratios of the untreated and surface densification and thermal post-treatment combined treated wood and discovered that hygroscopicity and radial swelling deformation are significantly decreased [12].

The HT process requires rigorous conditions; that is, relatively high temperature and long holding time under the oxygen-deficient environment (oxygen content below 3%). Since HT is a chemical-free process, the main modification mechanism is the autocatalytic reactions of the cell-wall constituents at high temperatures. Acetyl groups of the hemicellulose are partly cleaved, which leads to the formation of acidic intermediate products that further promote the changes of other chemical composition [17,23]. Lastly, the HT process does not make wood fireproof [28,29].

Nitrogen–phosphorus (NP) is an environmentally friendly, non-toxic, relatively inexpensive fire retardant [30]. Furthermore, the catalytic dehydration and catalytic charring of the NP wood fire resistance occurs between heating of 115 °C and 246 °C [31–33]. Hygroscopicity and low leachability resistance are possible limitations for a practical application of the NP, and studies for enhancing these properties can be found in published papers [29,31–33]. In former studies, NP has been used as an acidic-accelerating medium to intensify the effect of HT on wood. It brought about significant property improvement for the NP pre-impregnated and heated wood at a low treatment temperature for a short period of time [29,33]. More relevant studies also proved that acid pre-treatments can accelerate the thermal degradation of wood components and led to a treated wood moisture content lower than conventional HT, under the same treatment weight loss level [34,35].

There is a research gap regarding the effects of the NP fire retardant on THM densification of wood. In the present study, the NP fire retardant is used to reinforce poplar wood together with the thermal densification, aimed at fabricating a functionalized surface layer to enhance fire retardancy and compression stability of combined treated wood. This study provides a novel combined modification, which can functionalize the surface layer and endow multiple functions to the treated wood. It will be useful for promoting the usage of plantation timber.

2. Materials and Methods

2.1. Treatment

Poplar (*Populus beijingensis* W. Y. Hsu) at about 10% moisture content was purchased from a timber supplier in Beijing, China. Defect-free sapwood samples with length, width, and thickness of 300 mm × 150 mm × 19 mm, respectively, were prepared. All samples were polished with 240-grit sandpaper to ensure uniform surface roughness prior to modification. Then, they were divided into six groups (Table 1), each comprised of 15 samples.

Table 1. Treatment classes and the treatment condition of treated samples.

Groups	Pre-Treatment	Compression Ratios (%)	Compression Temperature (°C)
W_{NP-TM}	10% NP	21	180
W_{TM}	No	21	180
W_{HT-TM}	HT220	21	180
W_{HT}	HT220	No	No
W_{NP}	10% NP	No	No
W_C	No	No	No

Note: 10% NP means 10% nitrogen phosphorus fire-retardant aqueous solution impregnation; HT220 means heat treatment under 220 °C for 120 min.

The NP impregnation and HT conduction protocols were kept the same as in former studies [29,33]. Samples in groups W_{NP-TM} , W_{TM} , and W_{HT-TM} were pre-heated using a thermo-compressor (MLG68-S, Zhengzhou, China) for 5 min, then thermo-mechanically pressed to 14 mm final thickness using a stopper for 20 min at constant temperature.

2.2. Properties of the Functionalized Surface Layer

The surface colorimetric parameters were evaluated based on the CIELAB color coordinates using a photometry instrument (Dataflash 110 Datacolor, Lawrenceville, NJ, USA) with illuminant D65 and 10° standard observer. The mean values of five positions on each sample were recorded and the total color difference (ΔE^*) was calculated.

Five samples (50 mm × 50 mm × thickness) were cut from the middle of each of the untreated and treated groups. A vertical density profile tester (CreCon's X-ray densitometer, Martinsried, Germany) was used to measure the vertical density profile (VDP) of each sample and the average density profile was calculated. The average density profile accurately reflects density change throughout the sample thickness.

2.3. Compression Recovery via Soaking Test

Compression recovery was measured by soaking samples in a deionized water bath (20 ± 2 °C) for 120 min and then oven-drying. Their axial surfaces (20 mm × 20 mm × thickness) were covered by resin before the test. The thickness and surface hardness (HD) of each sample were measured before and after the soaking test. Thickness was measured three times from each sample at the center by digital caliper and HD was tested by a Shore D Hardness Tester (TH210, Beijing). All measurements were conducted after conditioning the samples to 10% equilibrium moisture content. Surface hardness recovery (HD_r) and thickness recovery (T_r) were calculated as follows:

$$HD = 100 - L/0.025 \quad (1)$$

$$HD_r = (HD_{fd} - HD_{fs}) / (HD_{fd} - HD_{bd}) \times 100\% \quad (2)$$

$$T_r = (T_{fd} - T_{fs}) / (T_{fd} - T_{bd}) \times 100\% \quad (3)$$

where L is the displacement of the needle when the pressure foot surface is in full contact with the sample surface; HD_{bd} and T_{bd} are the surface hardness and thickness before densification; HD_{fd} and T_{fd} are the surface hardness and thickness after densification; and HD_{fs} and T_{fs} are the surface hardness and thickness after soaking test.

2.4. Cone Analysis

Cone calorimeter tests were conducted according to ASTM 1354 (2004) with a cone calorimeter (FTT0242, West Sussex, UK). Three samples in the groups W_{NP-TM} , W_{TM} , W_{HT-TM} , and W_C were selected and wrapped with aluminum foil leaving a 100 mm square surface. During the test, the sample was exposed to a constant external heating flux, which was located at 250 mm over the surface, at an irradiance level of 50 kW m^{-2} .

2.5. Clustering and Morphological Analysis

Hierarchical cluster analysis (HCA) was performed using IBM SPSS Statistics 22.0 by between group linkage method [36]. The heat release and smoke production values from the cone test and compression recovery values from soaking test were taken into consideration, respectively. Microscopy and microanalysis of the groups W_C , W_{NP-TM} , W_{TM} , W_{HT-TM} , and W_{NP} were conducted with a SEM-EDS energy-dispersive X-ray spectrometer (JSM-6510, Tokyo, Japan). Samples were covered by galvanic gold deposition with an MC1000 ion sputter (FEI, Tokyo, Japan) working at a current of 5 mA for 45 s. All analyses were performed with 20 kV acceleration voltages.

3. Results and Discussion

3.1. Properties of the Functionalized Surface Layer

Photos and vertical density profile (VDP) curves are shown in Figure 1; the CIEL* a^* b^* and VDP values on different regions of the untreated and treated samples are shown in Table 2. It is evident that the W_{NP-TM} exhibits a uniform light-brown surface whereas the W_{TM} one presents a light surface. It can be deduced that the combined process could play an important role in the color generation of the NP-TM-treated wood because the merely NP impregnation process cannot change the surface color significantly [37].

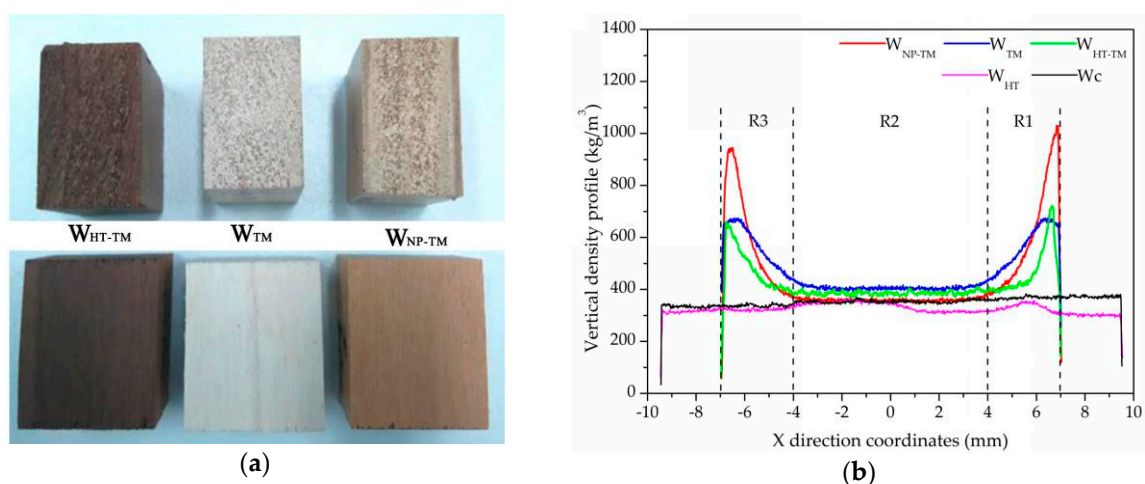


Figure 1. Photo (a) and vertical density profile (VDP) curves (b) of the selected samples.

Table 2. Color in CIE L* a* b* system and density of the selected samples.

Groups	Color in CIE L* a* b* System				Vertical Density Profile (kg m ⁻³)				
	L*	a*	b*	ΔE^*	R1	R2	R3	Maximum (× coordinate)	Average Value
W _{NP-TM}	54.99 ± 3.41	13.26 ± 1.68	29.19 ± 0.51	33.37 ± 1.38	675.68	365.48	569.97	1030.22 (6.83)	453.67
W _{TM}	80.33 ± 3.76	3.49 ± 0.60	21.40 ± 0.36	6.09 ± 2.03	578.65	410.62	567.90	673.43 (−6.43)	473.61
W _{HT-TM}	44.56 ± 1.07	9.36 ± 0.51	19.40 ± 0.43	40.21 ± 1.56	391.69	386.55	484.60	720.29 (6.66)	420.21
W _{HT}	47.18 ± 4.23	9.87 ± 0.42	20.80 ± 2.02	37.85 ± 2.72	297.25	330.58	313.76	365.29 (−1.74)	324.41
W _c	84.16 ± 5.79	2.95 ± 1.48	16.69 ± 1.83	-	372.18	354.10	331.02	382.76 (5.59)	352.38

According to Table 2, the a*, b*, and L* values of W_{TM} and W_{HT-TM} changed slightly compared with that of W_c and W_{HT}. That is to say, the only-TM process under 180 °C could not change the surface color of poplar wood. Interestingly, the b* and a* values of the W_{NP-TM} increased by 74.9% and 349.5%, respectively. The ΔE^* values of the W_{NP-TM} are higher than 33.37, further indicating that NP-TM treatment with relatively a short period (20 min) is quite sufficient for changing the color of poplar. After the NP-TM, poplar possessed a warmer and more attractive surface color, which is considered to be essential for furniture and interior decoration materials.

Figure 1b indicates that the VDP of untreated poplar was relatively uniform throughout the thickness with an average density of 352.38 kg/m³. The average density of W_{HT} decreased by 7.94% because of the thermal degradation of wood, which is consistent with some previous studies [17,22,38]. All the treated samples were divided into three regions according to the density changes; namely two surface layers (R1 and R3) and one core layer (R2). After the TM, the VDP values of the surface layers on W_{NP-TM}, W_{TM}, and W_{HT-TM} increased significantly. The NP-TM process brought the highest VDP values to the W_{NP-TM} on the surface layers, wherein the VDP value of R1 was 16.77% higher than that of W_{TM}. Meanwhile, the location of maximum VDP value on the W_{NP-TM} was closer to the surface and density of the R2 was almost kept the same level as W_c. However, the maximum VDP values of the W_{TM} and W_{HT-TM} were much lower than W_{NP-TM}, and compression was also affected in the core section. This indicates that the compression was mostly in the surface layer (about 3 mm). It has been reported that the NP has a catalytic dehydration effect on wood polysaccharides during HT [32], and this could also make the wood surface layer more likely to be compressed because of the softening effect at higher moisture and temperature conditions [25]. From NP fire retardants can be produced softener-NH₃, which reduces glass transition temperature of lignin, i.e., decrease T_g from approximately 170 °C [39]. Furthermore, the impregnated NP partly increased the density as most of it remained in the surface layer.

3.2. Compression Recovery of the Functionalized Surface Layer during Soaking Test

Normally, the compression state of TM wood is sensitive to moisture, which limits the usage of it to certain condition [12]. The thickness and surface hardness (*HD*) change of treated wood before and after the TM process, as well as compression recovery (*HD_r* and *T_r*), are displayed in Figure 2. The NP-TM treatment resulted in a better surface strength and the compression-fixing ability for poplar. W_{NP-TM} has higher *HD* value than that of W_{TM} before and after the water soaking test.

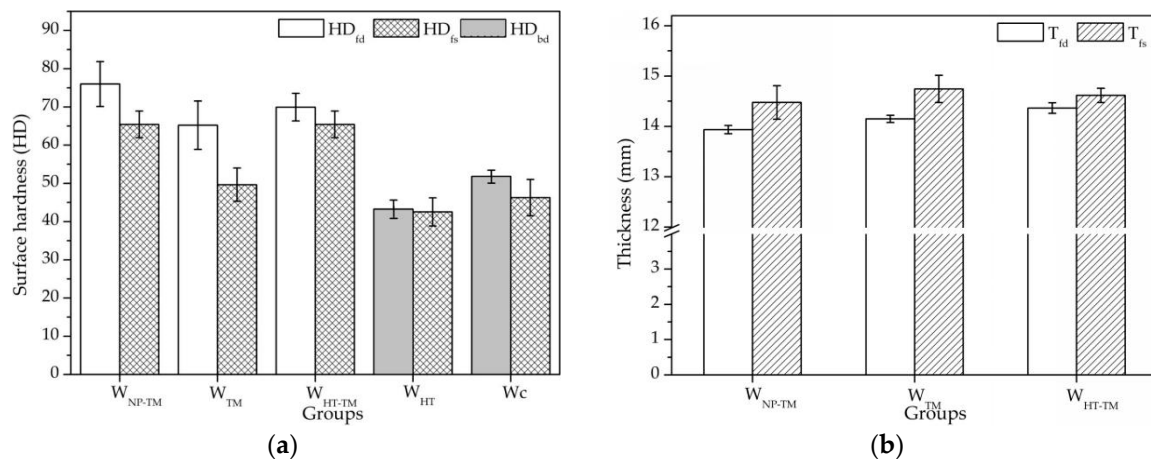


Figure 2. Surface hardness (a) and thickness changes (b) of selected samples.

Because of the TM, the HD_{fd} value of W_{TM} was 65.23, which is 20.59% higher than untreated poplar; the HD_{fd} value of W_{HT-TM} increased to 69.92, namely 61.66% higher than W_{HT} . After the NP-TM, the HD_{fd} values of W_{NP-TM} became 75.98, that is, 16.48% higher than W_{TM} . In other words, the NP-involving compression could cause larger surface hardness improvement on wood.

After water soaking test, all densified samples swelled to some extent, resulting in recovery of thickness and HD. Even for W_c , the surface hardness after soaking (HD_{fs}) decreased by 10.66% (Figure 2a). The W_{TM} had a poor compression ability; HD_r and T_r were the highest of all. The surface layer absorbed water and recovered to the status before the TM. While the W_{HT-TM} had the best compression ability, HD_r and T_r values of W_{HT-TM} were the lowest. The reason is that the HT increased the hydrophobicity and the TM process further enhanced the surface density of W_{HT-TM} . The compression stability of W_{HT-TM} samples remarkably enhanced due to the NP pre-treatment and the acceleration effect of NP on wood thermal degradation during the thermo-densification process [29,33]. When compared with that of W_{TM} , the HD_{fs} value was 31.60% higher and the T_r value decreased from 26.65% to 6.07%.

3.3. Effect of the Functionalized Surface Layer on Heat and Flue Gas Release via Cone Analyses

As shown in Figure 3 and Table 3, the W_{NP-TM} samples had the most moderate heat and flue gas release rate. W_{TM} and W_{HT-TM} samples were also enhanced by the TM process to some extent, especially in the preliminary stage of burning during the Cone test.

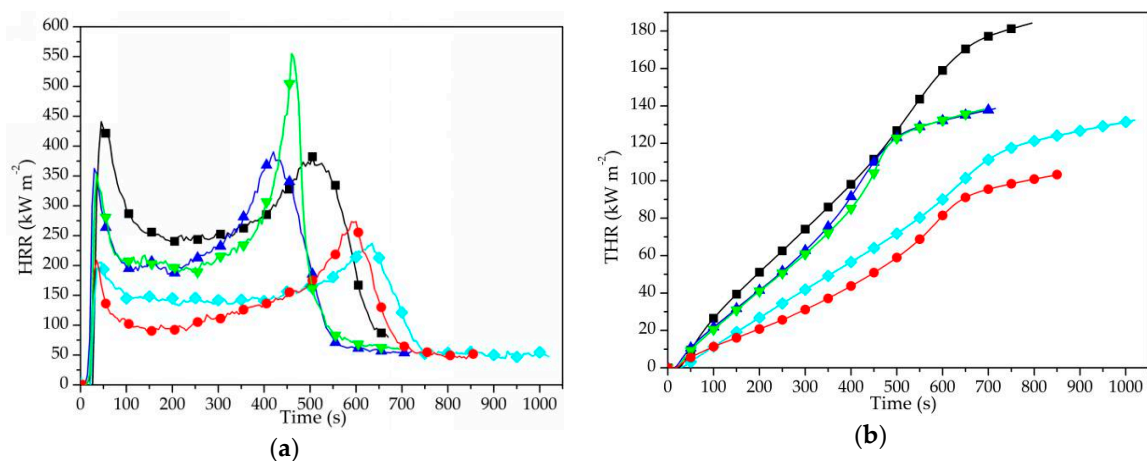


Figure 3. Cont.

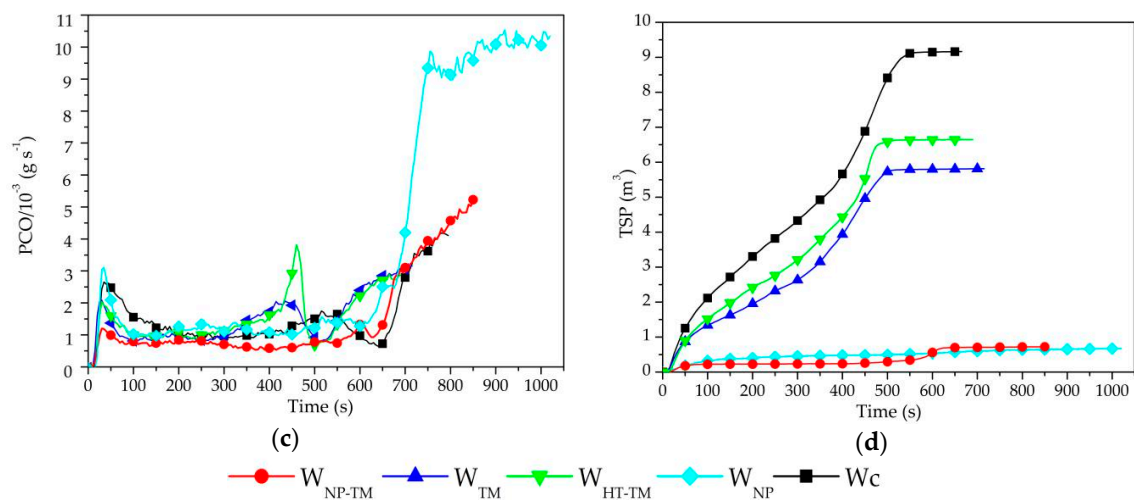


Figure 3. Heat release rate (a) and total heat release (b), generation rate of carbon monoxide (c), and total smoke production (d) of the selected samples.

Table 3. Heat release and flue gas release of selected samples during cone analysis.

Item	Groups				
	W_{NP-TM}	W_{TM}	W_{HT-TM}	W_{NP}	W_c
HRR (kW m^{-2})	122.49	196.54	204.57	131.69	236.08
THR (MJ m^{-2})	103.50	138.60	138.14	132.44	184.24
HRR (60 s) (kW m^{-2})	133.74	259.51	254.70	122.00	311.26
HRR (360 s) (kW m^{-2})	110.27	225.66	217.24	146.72	255.06
Peak HRR1 (kW m^{-2})	208.84	362.82	353.31	172.83	437.16
Peak HRR2 (kW m^{-2})	273.71	390.40	555.30	234.94	345.39
Time to Peak HRR1 (s)	30	25	30	45	45
Time to Peak HRR2 (s)	585	415	455	645	520
mean EHC (MJ kg^{-1})	14.64	21.83	21.03	18.78	27.38
TSP (m^2)	0.72	5.81	6.64	0.65	7.86
TSR ($\text{m}^2 \text{m}^{-2}$)	81.33	657.39	751.48	73.02	888.95
COY/ 10^{-3} (kg kg^{-1})	20.20	19.10	17.80	63.90	20.70
COY (60 s) / 10^{-3} (kg kg^{-1})	10.70	12.40	12.60	23.00	18.30
COY (360 s) / 10^{-3} (kg kg^{-1})	10.60	12.90	11.60	16.50	14.60
CO ₂ Y (kg kg^{-1})	1.29	1.96	1.88	1.59	2.37

Note: HRR, heat release rate; THR, total heat release; HRR (60 s), heat release rate within 60 s; HRR (360 s) heat release rate within 360 s; Peak HRR1, peak of the heat release rate at lower temperature; Peak HRR2, peak of the heat release rate at higher temperature; EHC, effective heat of combustion; TSP, total smoke production; TSR, total smoke release; COY, CO yield; COY (60 s), CO yield within 60 s; COY (360 s), CO yield within 360 s; CO₂Y, CO₂ yield.

The HRR curve in Figure 3a reveals that the W_c had two sharp exothermic peaks; the burning of combustible gas emitted by the decomposition of the surface formed the peak HRR1 at 45 s, then the oxidation reaction of internal wood material formed peak HRR2 at 520 s because of the consuming and cracking of the surface charcoal layer.

According to Table 3, the THR and TSP values of W_{TM} and W_{HT-TM} were decreased because of the TM process. However, the HRR curves of W_{TM} and W_{HT-TM} caught up with untreated wood and then reached the peak HRR2, which was 13.0% and 60.8% higher than that of W_c (Figure 3a,b). Furthermore, the time to peak HRR2 appeared 105 s and 65 s ahead; meanwhile, the surface cracking increased the CO release, as shown in Figure 3c. This could be explained that the higher density of formed charcoal provided a better protection for inner material at the initial stage, but the recovery of the compressed wood and cracking of surface charcoal under high temperature cause a more violent combustion reaction. Therefore, the TM treatment may also bring potential risk to the treated wood.

Compared with that of W_c , the HRR curve of W_{NP-TM} declined remarkably in the whole combustion process. The peak $HRR1$ decreased by 52.2% and appeared 15 s ahead, then remained at a continuously lower HRR value. It points to the fact that the W_{NP-TM} formed a protective surface charcoal rapidly with less heat release and the resistance of the charcoal layer enhanced. Different from the simply TM wood, the NP-TM process made the W_{NP-TM} more stable during the burning. The extent of surface cracking on W_{NP-TM} was much lower; the peak $HRR2$ decreased by 29.9% and 50.7%, and the relevant time delayed for 170 s and 130 s, when compared with that of W_{TM} and W_{HT-TM} . It is worth mentioning that the THR , TSP , and COP values of W_{NP-TM} were also lower than solely NP-treated wood.

The NP-TM made the surface layer of W_{NP-TM} denser, which could be in favor of the oxygen and heat insulation performances of treated wood. Hence, the generation rate of CO and total smoking production were the lowest within the first 600 s. The surface cracking occurred at the faint-flame stage and increased the contact of charcoal with oxygen. The CO release declined sharply at about 600 s and then kept a relatively lower level after 700 s. In other words, the swelling of densified wood and cracking of surface charcoal could be effectively controlled by the NP-TM method. The enhancement could be explained by the synergistic effects of density-increase and carbon-forming by NP fire retardant. Therefore, it can be concluded that the fire retardancy of the W_{NP-TM} was significantly improved by the functionalized surface layer.

3.4. Compression Recovery of the Functionalized Surface Layer during Cone Analyses

In order to uncover the surface compression recovery of the treated wood during burning and its effects on the smoke release, the correlation between the HRR and specific mass loss rate (SMLR), carbon monoxide yield (CO yield), and smoke production rate (SPR) in different stages were also taken into account, as shown in Figure 4.

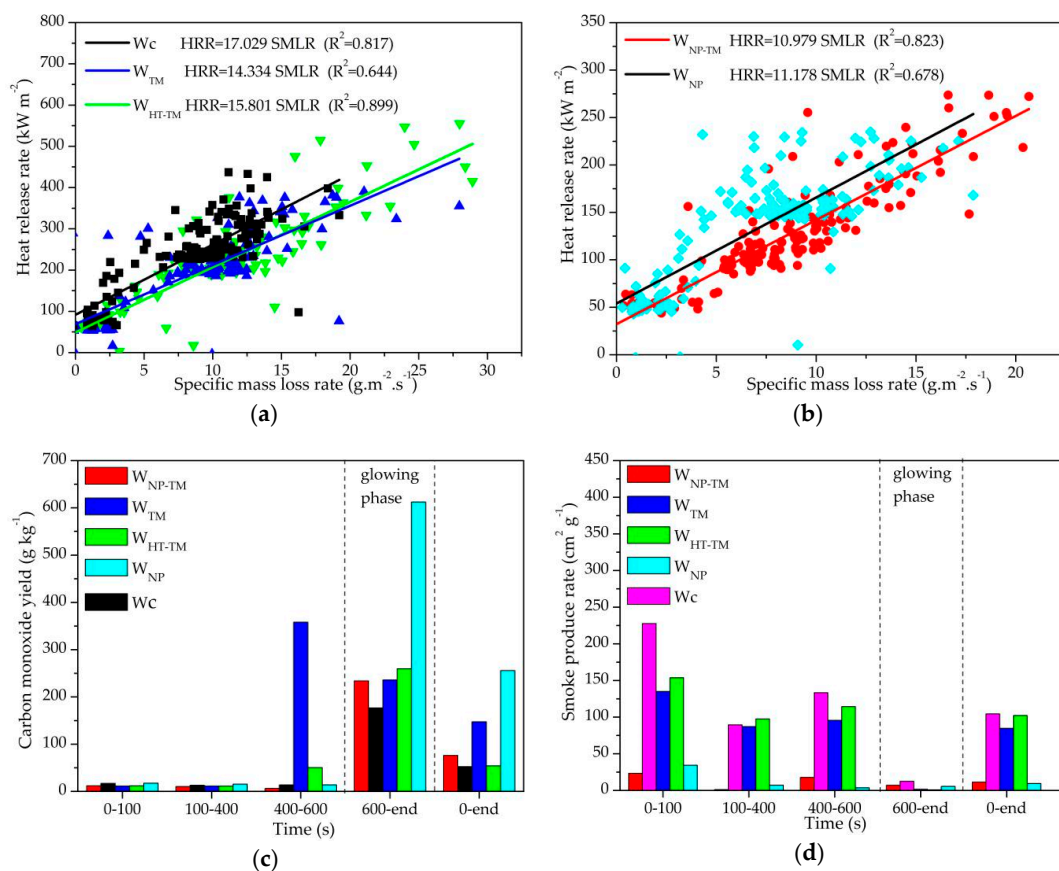


Figure 4. Correlation of heat release rate with specific mass loss rate (a, b), the CO yield (c), and smoke production rate (d) of the selected samples.

Equations of the linear statistical dependence of the *HRR* on the specific mass loss rate are listed in Figure 4a,b. Under perfect combustion, the *HRR* is a function of specific mass loss rate only ($R^2 = 1$); the slope of fitting line was the smallest and the R^2 value of W_{NP-TM} was much higher than that of W_{NP} , showing that the W_{NP-TM} possesses higher combustion efficiency. Considering the lowest *mean EHC* (Table 3) and lowest heat release (Figure 3a,b), it can be concluded the combustion reaction of W_{NP-TM} was the most moderate and stable.

The oxygen-deficient combustion produces more CO; the main emission stage is faint flame combustion (glowing phase) of surface charcoal, after nearly 600 s (Figures 3c and 4c). The imperfect combustion causes more smoke release; the main emission stage is the flame combustion stage (Figures 3d and 4d).

Taking an overall consideration of the cone testing results, we can find that surface cracking of W_{TM} and W_{HT-TM} occurred at high temperature, resulted in shifting forward of the Peak *HRR*₂ (Figure 3a) and CO release (Figure 3b). Therefore, the surface cracking of W_{TM} and W_{HT-TM} was before 400 s and 450 s. The peak of CO release appeared with the surface cracking, caused by the anoxic burning of the inner material. Similarly, the surface cracking of W_{HT-TM} was around 600 s, closing to the glowing phase. As shown in Figure 4c, the CO yield of W_{TM} and W_{HT-TM} started to increase from the interval of 400–600 s, and it started after 600 s in case of the W_{NP-TM} .

It is worth noting that the CO release of W_{HT-TM} declined sharply after the surface cracking and kept the same level as W_c , much lower than that of W_{NP} . This could be explained by the fact that most of the inner materials have transformed into charcoal under protection of the functionalized surface layer, then the surface cracking of W_{NP-TM} took place in the glowing stage and increased the oxygen-contact area of char surface. This indicates that the NP-TM process enhanced the compression stability as well as CO inhibition of the treated wood in the high-temperature condition.

The surface layer of W_{NP-TM} was filled with NP fire retardant and compressed to a high density, which has an accelerating effect on the formation of charcoal and strengthening effect on the protective char layer at the early stage of burning. Then, the compression-stable charcoal protected the inner material from burning because of the heat or oxygen-barrier properties. Therefore, the heat and CO release of W_{NP-TM} declined and the surface cracking delayed when compared with that of W_{TM} . At the glowing stage, the surface cracking increased the oxygen contact and reduced CO release from oxidization of charcoal (Figures 3c and 4c).

3.5. Clustering and SEM-EDS Analysis

Cluster analysis of the NP-TM and untreated samples was done based on values of color in CIE $L^*a^*b^*$ system (Table 2), heat release and flue gas release (Table 3), and compression recovery (Figure 2); the dendrogram of those clusters is shown in Figure 5.

The dendrogram of HCA for treated samples in regard to surface color (Figure 5a) shows two main clusters; the W_{NP-TM} was classified into the first group, which also contains W_{HT} and W_{HT-TM} , while the W_c and W_{TM} were classified into the second group, further proving that the NP-TM process can lead to color generation.

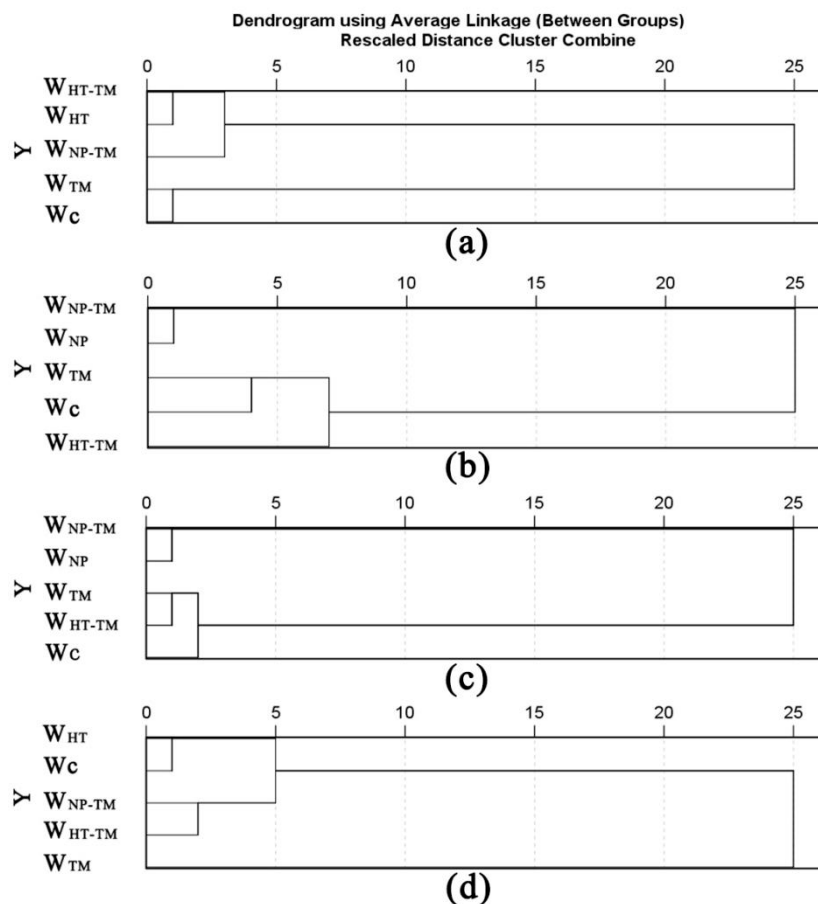


Figure 5. Hierarchical cluster analysis (HCA) of surface color (a), heat release (b), flue gas release (c), and compression recovery (d) based on different variables. Note: The horizontal axis shows the distances of clusters and the vertical axis shows combine treatment and the control group.

In terms of dendrogram for heat release (Figure 5b) and flue gas release (Figure 5c), it is observed that the W_{NP-TM} was classified into the same group with the W_{NP} . It verified that the functionalized surface layer, created by NP-TM process, can endow the treated wood with flame retardant and smoke suppression properties. However, the only-TM treatment could not render raw poplar or heat-treated poplar fireproof. This result is in accordance with that of the cone analyses discussed in Sections 3.3 and 3.4. For the compression recovery, dendrogram of HCA are grouped into two blocks: W_{TM} and other groups. The first cluster was separated into two subgroups (Figure 5d). The compression recovery improvement of the W_{NP-TM} could elucidate that the NP fire retardant acts as an acid accelerator, which could intensify the effectivity of HT [29,33], as the W_{HT-TM} and W_{NP-TM} are classified into the same subgroups.

The SEM micrographs and EDXA spectra of untreated and NP-TM-treated samples are displayed in Figure 6.

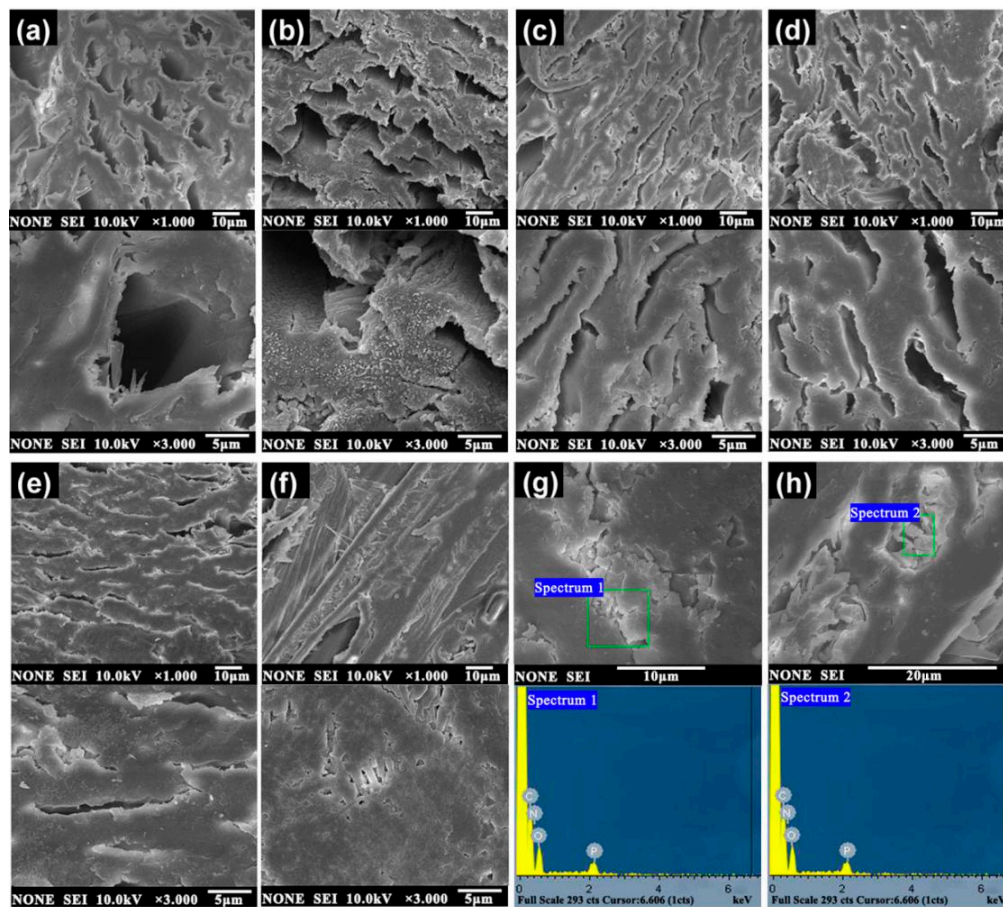


Figure 6. Scanning electron microscopy (SEM) micrographs of treated samples: (a) W_c ; (b) W_{NP} ; (c) W_{TM} ; (d) W_{HT-TM} ; (e) W_{NP-TM} on transverse section; (f) W_{NP-TM} on tangential section; (g,h) energy-dispersive X-ray analysis (EDXA) spectra of W_{NP-TM} .

The wood cell wall structure of W_c was intact and the inner faces are flat and smooth. After the TM, cell lumens (particularly distinct in the vessels) of W_{TM} and W_{HT-TM} samples were deformed, and the volume of void spaces declined sharply. However, the lumens of W_{TM} were partly open and had many fractures on the cell walls. This could increase the water absorption and cell wall swelling, finally causing compression recovery. The W_{HT-TM} also had some fractures on the cell walls, while the less hydrophilic caused by HT process could prevent it from swelling and recovery [40].

For the W_{NP} , the NP fire retardant distributed over the inner surface separately, as represented in Figure 6b. Because of the NP-TM process, it is quite clear that a large number of vessels are almost closed up and the cell walls are deformed on the W_{NP-TM} . Moreover, there are a few fractures that occurred on the cell walls (Figure 6e). According to Figure 6g,h, some crystalline particles fill between small gaps on the cell wall, and the crystallized-substance integrated the compressed and flattened cell lumens of the W_{NP-TM} . EDXA spectra further confirm that the filler gathered in pore spaces both on transverse (Figure 6g) and tangential (Figure 6h) sections is composed of NP fire retardant. It is speculated that the low molecular ammonium polyphosphate (APP) in NP fire retardant decomposed during the TM process and the intermediate products like H_3PO_4 further promote the catalytic dehydration of wood polysaccharides and enhanced the plasticity of the cell walls. Furthermore, the NP entered micro-voids, forming a connective crystal between the cell walls. Compared to that of W_{NP} , the connection of the NP and cell walls transform from particle to cementing, which will probably be another nonnegligible factor for the enhance of fire resistance and compression stability.

4. Conclusions

This work investigated the fire resistance and compression recovery properties of the treated poplar with a functionalized surface layer, formed by a novel combined treatment of nitrogen–phosphorus fire retardant (NP) pre-impregnation and thermo-mechanical densification (TM). Based on the findings of this study, the combined process could improve the surface aesthetics, fire retardancy, and compression stability of poplar wood. The NP accelerated the thermal degradation of wood and transformed to connective crystal between wood cell walls and cell lumens. This functionalized surface layer is composited by the degradation products of NP and wood. It possesses a superiority of high density and compression stability. The heat release rate of the combined treated wood is 48.1% lower than that of untreated wood, and the CO yield is 68.4% lower than that of only-NP-treated wood. Moreover, the compression recovery in the thickness is 77.2% lower than that of solely TM-treated wood. This study provides a new approach to enhance both fire resistance and compression stability of wood by fabricating a functional surface layer. Further studies in terms of controlling the formation and performance of the surface layer will be of interest in the future.

Author Contributions: Conceptualization, D.C. and J.M.; Methodology, D.C. and J.M.; Software, D.C. and S.R.; Validation, J.M., S.A., and S.L.; Formal Analysis, D.C., J.M., and Z.L.; Investigation, D.C. and J.M.; Resources, D.C. and J.M.; Data Curation, D.C., S.R., and J.M.; Writing–Original Draft Preparation, D.C.; Writing–Review & Editing, J.M., S.A., S.L., S.R., and Z.L.; Visualization, D.C.; Supervision, J.M. and S.A.; Project Administration, J.M.; Funding Acquisition, J.M.

Funding: This research was funded by the Forestry Public Welfare Project Foundation of China, grant number 201404502, and the Fundamental Research Funds for the Central Universities of China, grant number 2015ZCQ-CL-01.

Conflicts of Interest: The authors declare no conflict of interest.

References

- Hill, C.A.S. *Wood Modification, Chemical, Thermal and Other Processes*; John Wiley & Sons: Chichester, UK, 2006.
- Quiroga, A.; Marzocchi, V.; Rintoul, I. Influence of wood treatments on mechanical properties of wood–cement composites and of *Populus Euroamericana* wood fibers. *Compos. B Eng.* **2016**, *84*, 25–32. [[CrossRef](#)]
- Yuan, Q.P.; Su, C.W.; Xiong, J.B. Research Progress of Plantation Wood Machining Properties. *J. Anhui Agric. Sci.* **2011**, *3*, 42–45.
- Lin, H.; Wang, Y.; Chen, Z.D.; Yang, B.X. Progress & Application Prospects of Modified Wood. *For. Mach. Woodwork. Equip.* **2006**, *34*, 11–13.
- Kiaei, M.; Naji, H.R.; Abdul-Hamid, H.; Farsi, M. Radial variation of fiber dimensions; annual ring width; and wood density from natural and plantation trees of alder (*alnus glutinosa*) wood. *Drev. Vysk. Wood Res.* **2016**, *61*, 55–64.
- Bekhta, P.; Proszyk, S.A.; Krystofiak, T. Colour in short-term thermo-mechanically densified veneer of various wood species. *Eur. J. Wood Prod.* **2014**, *72*, 785–797. [[CrossRef](#)]
- Kwon, J.H.; Shin, R.; Ayrilmis, N.; Han, T.H. Properties of solid wood and laminated wood lumber manufactured by cold pressing and heat treatment. *Mater. Des.* **2014**, *62*, 375–381. [[CrossRef](#)]
- Büyüksarı, U. Surface characteristics and hardness of MDF panels laminated with thermally compressed veneer. *Compos. B Eng.* **2013**, *44*, 675–678. [[CrossRef](#)]
- Song, J.; Chen, C.; Zhu, S.; Zhu, M.; Hu, L. Processing bulk natural wood into a high-performance structural material. *Nature* **2018**, *554*, 224–228. [[CrossRef](#)]
- Diouf, P.N.; Stevanovic, T.; Cloutier, A.; Fang, C.; Blanchet, P.; Koubaa, A.; Mariotti, N. Effects of thermo-hygro-mechanical densification on the surface characteristics of trembling aspen and hybrid poplar wood veneers. *Appl. Surf. Sci.* **2011**, *257*, 3558–3564. [[CrossRef](#)]
- Laine, K.; Segerholm, K.; Walinder, M.; Rautkari, L.; Hughes, M. Wood densification and thermal modification, hardness; set-recovery and micromorphology. *Wood Sci. Technol.* **2016**, *50*, 883–894. [[CrossRef](#)]
- Zhan, J.; Avramidis, S. Needle fir wood modified by surface densification and thermal post-treatment, hygroscopicity and swelling behavior. *Eur. J. Wood Prod.* **2016**, *74*, 49–56. [[CrossRef](#)]

13. Darwis, A.; Wahyudi, I.; Dwianto, W.; Cahyono, T.D. Densified wood anatomical structure and the effect of heat treatment on the recovery of set. *J. Indian Acad. Wood Sci.* **2017**, *1–8*. [[CrossRef](#)]
14. Chen, A.T.; Luo, P.P.; Xu, Z.Y.; Hu, Z.J. Effects of furfuryl alcohol impregnation on physical and mechanical properties of densified poplar wood. *J. For. Eng.* **2016**, *1*, 21–25. [[CrossRef](#)]
15. Dömény, J.; Čermák, P.; Koiš, V.; Tippner, J.; Rousek, R. Density profile and microstructural analysis of densified beech wood (*Fagus sylvatica* L.) plasticized by microwave treatment. *Eur. J. Wood Prod.* **2017**, *1–7*. [[CrossRef](#)]
16. Laine, K.; Segerholm, K.; Wälinder, M.; Rautkari, L.; Hughes, M.; Lankveld, C. Surface densification of acetylated wood. *Eur. J. Wood Prod.* **2016**, *74*, 829–835. [[CrossRef](#)]
17. Gu, L.B.; Ding, T.; Jiang, N. Development of wood heat treatment research and industrialization. *J. For. Eng.* **2019**, *4*, 1–11. [[CrossRef](#)]
18. Salca, E.; Hiziroglu, S. Evaluation of hardness and surface quality of different wood species as function of heat treatment. *Mater. Des.* **2014**, *62*, 416–423. [[CrossRef](#)]
19. Ding, T.; Peng, W.W.; Li, T. Mechanism of color change of heat-treated white ash wood by means of FT-IR and XPS analyses. *J. For. Eng.* **2017**, *4*, 25–30. [[CrossRef](#)]
20. Altgen, M.; Willems, W.; Hosseinpourpia, R.; Rautkari, L. Hydroxyl accessibility and dimensional changes of Scots pine sapwood affected by alterations in the cell wall ultrastructure during heat-treatment. *Polym. Degrad. Stab.* **2018**, *152*, 244–252. [[CrossRef](#)]
21. Zhang, N.N.; Xu, M. Effects of silicon dioxide combined heat treatment on properties of rubber wood. *J. For. Eng.* **2019**, *4*, 38–42. [[CrossRef](#)]
22. Wei, Y.X.; Zhang, P.; Liu, Y.; Chen, Y.; Gao, J.M.; Fan, Y.M. Kinetic analysis of the color of larch sapwood and heartwood during heat treatment. *Forests* **2018**, *9*, 289. [[CrossRef](#)]
23. Sundqvist, B.; Karlsson, O.; Westermarck, U. Determination of formic-acid and acetic acid concentrations formed during hydrothermal treatment of birch wood and its relation to colour; strength and hardness. *Wood Sci. Technol.* **2006**, *40*, 549–561. [[CrossRef](#)]
24. Gaff, M.; Babiak, M.; Kačík, F.; Sandberg, D.; Turčani, M.; Hanzlík, P.; Vondrová, V. Plasticity properties of thermally modified timber in bending-The effect of chemical changes during modification of European oak and Norway spruce. *Compos B Eng.* **2019**, *165*, 613–625. [[CrossRef](#)]
25. Fang, C.H.; Cloutier, A.; Blanchet, P.; Koubaa, A. Densification of wood veneers combined with oil-heat treatment. Part I, Dimensional stability. *BioRES* **2011**, *6*, 373–385. [[CrossRef](#)]
26. Fang, C.H.; Cloutier, A.; Blanchet, P.; Koubaa, A. Densification of wood veneers combined with oil-heat treatment. Part II, hygroscopicity and mechanical properties. *BioRES* **2012**, *7*, 925–935. [[CrossRef](#)]
27. Avila, C.B.; Escobar, W.G.; Cloutier, A.; Fang, C.H.; Carrasco, P.V. Densification of wood veneers combined with oil-heat treatment. Part III, cell wall mechanical properties determined by nanoindentation. *BioRES* **2012**, *7*, 1525–1532. [[CrossRef](#)]
28. Şahin, K.H.; Yusuf, S. The thermal conductivity of fir and beech wood heat treated at 170; 180; 190; 200; and 212°C. *J. Appl. Polym. Sci.* **2011**, *121*, 2473–2480. [[CrossRef](#)]
29. Chu, D.M.; Mu, J.; Zhang, L.; Li, Y.S. Promotion effect of NP fire retardant pre-treatment on heat-treated poplar wood. Part 1, color generation; dimensional stability; and fire retardancy. *Holzforschung* **2017**, *71*, 207–215. [[CrossRef](#)]
30. Yu, L.P.; Li, G.P. Study on processing conditions of spruce with nitrogen-phosphorus-boron environmentally friendly fire retardant. *China Wood Based Panels* **2006**, *13*, 14–16.
31. Gu, B. Study on the Effect of Properties of UF Plywood Treated with BL-Environmental Friendly Flame Retardant. Chapters, Composition Analysis of BL Environmental Protection Flame Retardant. Ph.D. Thesis, Beijing Forestry University, Beijing, China, 2007; pp. 50–56.
32. Zhang, X.T.; Mu, J.; Chu, D.M.; Zhao, Y. Synthesis of fire retardants based on N and P and poly(sodium silicatealuminum dihydrogen phosphate) (PSADP) and testing the flame-retardant properties of PSADP impregnated poplar wood. *Holzforschung* **2015**, *70*, 341–350. [[CrossRef](#)]
33. Chu, D.M.; Mu, J.; Zhang, L.; Li, Y.S. Promotion effect of NP fire retardant pre-treatment on heat-treated poplar wood. Part 2, hygroscopicity; leaching resistance; and thermal stability. *Holzforschung* **2017**, *71*, 217–223. [[CrossRef](#)]
34. Hosseinpourpia, R.; Adamopoulos, S.; Mai, C. Effects of Acid Pre-Treatments on the Swelling and Vapor Sorption of Thermally Modified Scots Pine (*Pinus sylvestris* L.) Wood. *BioRES* **2018**, *13*, 331–345. [[CrossRef](#)]

35. Himmel, S.; Mai, C. Effects of acetylation and formalization on the dynamic water vapor sorption behavior of wood. *Holzforschung* **2015**, *69*, 633–643. [[CrossRef](#)]
36. Guo, F.; Huang, R.F.; Lu, J.X.; Chen, Z.J.; Cao, Y.J. Evaluating the effect of heat treating temperature and duration on selected wood properties using comprehensive cluster analysis. *J. Wood Sci.* **2014**, *60*, 255–262. [[CrossRef](#)]
37. Li, S.J.; Qian, X.R.; Yu, J.; Wang, Q.W. Influence of FRW Fire Retardant Treatment on the Color and Painting Properties of Wood. *J. Northeast. For. Univ.* **1999**, *6*, 38–40.
38. Boruvka, V.; Zeidler, A.; Holecek, T.; Dudík, R. Elastic and Strength Properties of Heat-Treated Beech and Birch Wood. *Forests* **2018**, *9*, 197. [[CrossRef](#)]
39. Ladislav, R. *Wood Deterioration, Protection and Maintenance*; John Wiley & Sons: Chichester, UK, 2016.
40. Wang, W.; Zhu, Y.; Cao, J.Z.; Sun, W.J. Correlation between dynamic wetting behavior and chemical components of thermally modified wood. *Appl. Surf. Sci.* **2015**, *324*, 332–338. [[CrossRef](#)]



© 2019 by the authors. Licensee MDPI, Basel, Switzerland. This article is an open access article distributed under the terms and conditions of the Creative Commons Attribution (CC BY) license (<http://creativecommons.org/licenses/by/4.0/>).